Accelerated, decelerated, and oscillating fronts in a globally coupled bistable semiconductor system

M. Meixner, P. Rodin,* and E. Schöll
Institut für Theoretische Physik, Technische Universität Berlin, Hardenbergstrasse 36, D-10623 Berlin, Germany
(Received 31 March 1998)

We study front propagation in a globally coupled bistable semiconductor system. The analysis is based on an activator-inhibitor model derived for a gate-driven *pnpn* structure that is globally coupled via a gate-cathode circuit, but the model is applicable for more general cases of a spatially extended system with Z-shaped bistability. We demonstrate that a global constraint allows for efficient control over the front propagation. In the voltage-driven regime the front propagates with a constant speed whose value and direction are controlled by the gate potential. Under general gate circuit conditions the front dynamics experiences either a positive or a negative feedback which acts with adjustable delay. This allows for tuning between accelerated, decelerated, and oscillating fronts. [S1063-651X(98)12408-X]

PACS number(s): 05.70.Ln, 72.20.Ht, 85.30.−z

I. INTRODUCTION

Solid-state-based bistable or excitable active media with local or global inhibition [1] have attracted much interest in recent years. Current instabilities, pattern formation, and complex spatiotemporal dynamics have been studied in semiconductors and semiconductor devices [2–6], and especially in layered semiconductor structures like *pin* diodes [7,8], heterostructure hot electron diodes [9,10], resonant tunneling diodes [11–13], *pnp* (transistor) structures [4], *pnpn* (thyristor) structures [14–18], and $p^+npn^-n^+$ structures [19–23]. There is a high potential of expected applications of such active spatially extended media for information processing and pattern recognition [24,25]; this implies spatially inhomogeneous dynamical modes of operation and therefore the prospects essentially depend on the invention of efficient methods for controlling nonlinear spatiotemporal patterns. In this paper we address the problem of global control over front propagation in bistable extended media, focusing on gate-driven *pnpn* structures. Bistable *pnpn* structures not only exhibit a great variety of different spatiotemporal patterns, e.g., solitary filaments [26,16,17], front propagation [27,18], Turing patterns [14,15,18], but also possess unique features with respect to controllability. These features are introduced by a spatially distributed microelectronic gate which allows one to influence the internal state uniformly over the whole cross section of the device [16,17]. In this case, in addition to the global coupling through the main circuit, which occurs in all spatially distributed semiconductor systems [28–30] and has been studied in our previous paper [31], a global coupling through the gate circuit arises [16,17]. The external control circuit imposes a global constraint on the internal dynamics and provides means for control over spatiotemporal patterns. Recently, active external circuits with negative resistance and capacitance have been implemented in experimental studies of multistable structures [11]. This makes the control of semiconductor systems via a global constraint even more flexible since it allows us to arrange global constraints of both activator and inhibitor types.

If a bistable *pnpn* structure is switched from the low-conductivity to the high-conductivity state, a switching front triggers double injection from cathode and anode increasing the concentration of excess carriers up to ten orders of magnitude. This results in a dramatic increase of both conductivity and light emission providing a basis for numerous electrical and optical applications. Originally these applications were seen mainly in the field of power electronics [32], but nowadays *pnpn* structures attract attention as a prominent example of controllable solid-state-based active media which can serve as hardware for electrical [33] and optical [34] pattern recognition systems. An implementation of the principles of autowave holography for information processing [35] demands for controllable distributed media which exhibit both front propagation and solitary patterns [36]. Multilayered *pnpn* structures are promising candidates for single-crystal realizations of such media. In laser *pnpn* structures control of switching fronts means control of the active area of the semiconductor laser, which could be of great importance for optical systems.

In this paper we theoretically study the basic features of front propagation in a *pnpn* structure globally coupled via a gate-cathode circuit. We consider a *pnpn* structure (Fig. 1) whose design is similar to the single element of a modern gate-turn-off thyristor (e.g., [32]). It consists of a main circuit (K-A) connected to a bias voltage U, and a control circuit including an applied voltage u_0, resistance R, and external capacitance C_{ext}. The structure can be switched on or off locally by applying a voltage to one of the lateral gates G_1 and G_2. For appropriate parameters such local switching leads to the excitation of a front between high-current and low-current regions moving along the x direction. Our aim is to demonstrate that its dynamics can be controlled by means of the spatially extended gate G. The gate-driven *pnpn* structure can be described by the reaction-diffusion equation

$$\tau_a \frac{\partial a(x,t)}{\partial t} = l^2 \frac{\partial^2 a(x,t)}{\partial x^2} + f(a,u,U), \tag{1}$$

*On leave from A. F. Ioffe Physicotechnical Institute, Russian Academy of Science, 194021 St. Petersburg, Russia.

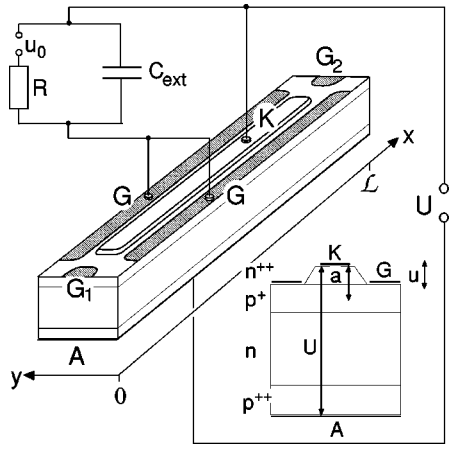

FIG. 1. Sketch of the gate-driven $p^{++}np^{+}n^{++}$ structure and the external circuit. The potential drops between the cathode K and the p^{+} layer, the gate G, and the anode A are denoted by a, u, and U, respectively (see inset showing a cross section of the structure).

with a nonlinear local kinetic function [16]

$$f(a,u,U) \equiv -\alpha a + \exp\, a - \beta\, \exp(-U+2a) + \gamma U + \kappa u. \tag{2}$$

Here $a(x,t), u(t), U(t)$ are the p-base potential, gate potential, and cathode-anode voltage, respectively (a, u, and U are measured in units of kT/e and are therefore dimensionless). The characteristic length l and the coefficients α, β, γ, κ of the local kinetic function are determined by the structural parameters [16], τ_a is the characteristic relaxation time of a. We are interested in the x dependence of the internal state $a(x,t)$ of the semiconductor structure, assuming it to be homogeneous along the y direction. Neumann boundary conditions are imposed on $a(x,t)$.

The nonpolynomial local kinetic function $f(a,u,U)$, has been derived from charge conservation and transport equations in [16]. The potentials u and U play the role of parameters with respect to the bistable medium. Physically, bistability of a $pnpn$ structure is associated with a change of the central (collector) $p^{+}n$-junction bias which is negative in the off state and becomes positive as the structure is switched on. This local kinetic function combines linear terms, corresponding to the leakage current of pn junctions which makes a major contribution to charge transport in the off state, and highly nonlinear exponential terms, corresponding to injection currents of the collector and emitter pn junctions, respectively [16]. The latter dominate in the on state, but the small prefactor β makes them negligible in the off state. That leads to the sharp rise of the local kinetic function (Fig. 2). Since the first term in Eq. (2) takes into account Ohmic conductances of both the gate contact and the emitter $n^{++}p^{+}$ junction, whereas the last term contains the latter contribution only, we generally have $\alpha > \kappa$ which is important for the following analysis.

We assume a voltage-controlled main circuit $U=\text{const}$ and impose one global constraint corresponding to the control circuit [37]:

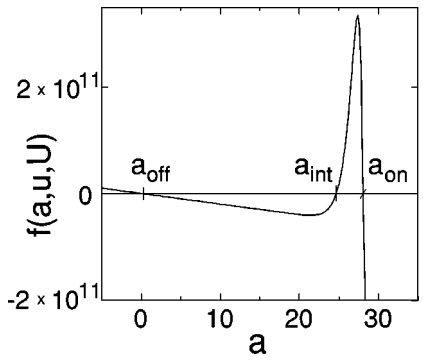

FIG. 2. The local kinetic function $f(a,u,U)$ (dimensionless). The off, intermediate, and on states are denoted by a_{off}, a_{int}, and a_{on}, respectively. The values of u and U are chosen as $u=0$ and $U=30.75$ satisfying the equal areas rule $\int_{\text{off}}^{\text{on}} f(a,u,U)da=0$. The numerical parameters $\alpha=2\times10^{9}$, $\beta=14.5$, $\gamma=10^{7}$, $\kappa=10^{9}$ correspond to a realistic $pnpn$ structure [26]. All potentials a, u, and U are in units of kT/e.

$$\tau_u \frac{du}{dt} = u_0(t) - u - R\int_0^{\mathcal{L}} j(a,u)dx, \quad \tau_u = RC,$$

$$C = C_{\text{int}} + C_{\text{ext}}. \tag{3}$$

Here $\mathcal{L}$ is the system length along the x direction, C_{int} is the differential cathode-gate capacitance of the device, C_{ext} has the meaning of a differential capacitance of the external circuit. For the current density per unit length between the gate and the cathode the following Ohmic dependence with conductivity σ is assumed:

$$j(a,u) = \sigma(u-a). \tag{4}$$

In the following we assume that t and x are measured in units of τ_a and l, respectively ($t \to t/\tau_a$, $x \to x/l$), which reduces Eqs. (1) and (3) to

$$\dot{a} = a'' + f(a,u,U), \tag{5}$$

$$\epsilon \dot{u} = u_0 - (1+\omega)u + \omega\langle a\rangle, \tag{6}$$

where the dot and the prime denote the derivatives with respect to t and x, respectively, and

$$\langle a\rangle \equiv \frac{1}{\mathcal{L}}\int_0^{\mathcal{L}} a(x)dx, \quad \epsilon \equiv \frac{\tau_u}{\tau_a}, \quad \omega \equiv \frac{R}{r}, \quad r \equiv (\mathcal{L}\sigma)^{-1}. \tag{7}$$

Note that r has the meaning of total internal resistance of the gate contact. All variables we use in the following are dimensionless.

The null isocline $a(u)$ of Eq. (5) defined by $f(a,u,U)=0$ is S-shaped for sufficiently large values of the main voltage $U > U_{\text{cr}}$ [Fig. 3(a)]. The steady-state current-voltage characteristic $j(u) \equiv j(a(u),u)$ of the gate current which results from the dependences $a(u)$ and $j(a,u)$ is Z-shaped [Fig. 3(b)]. Current-voltage characteristics of this type have been found recently in the double-barrier resonant-tunneling diode (DBRTD) [11]. Note that in contrast to the DBRTD gate-driven $pnpn$ structures are three-terminal devices

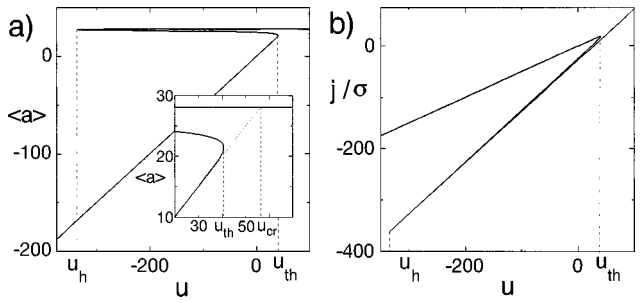

FIG. 3. (a) Null isocline $a(u)$ given by the local kinetic function $f(a,u,U)=0$ and (b) Z-shaped local current density vs voltage characteristic $j(u)$ for $U=30.75$ (a, u, U, and j/σ are in units of kT/e). The lower branch *off* of the $a(u)$ relation corresponds to the upper branch of $j(u)$ and vice versa. The holding voltage u_h and the threshold voltage $u_{\rm th}$ denote the left and right boundaries of the bistability regime. The inset in (a) shows the turning point at $u_{\rm th}$ and the voltage $u_{\rm cr}$ defined by Eq. (29) in an enlarged scale.

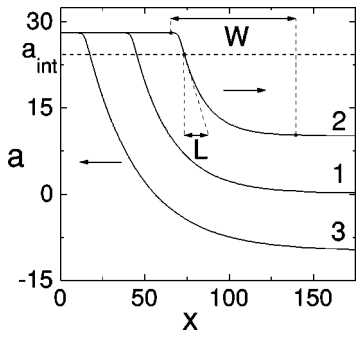

FIG. 4. The spatial profiles of the stationary front (curve 1, $u=0$), hot front (curve 2, $u=u_{\rm th}/2$), and cold front (curve 3, $u=-u_{\rm th}/2$). The front width W and the characteristic length L defined by Eq. (11) are indicated. The system length is $\mathcal{L}=1000$ (a and x are in units of kT/e and l, respectively).

which have a Z-shaped cathode-gate characteristic and an S-shaped cathode-anode characteristic. These different nonlinearities are associated with control and main circuits, respectively, and the Z subsystem is used to control the S subsystem. Stationary and moving kinklike patterns in the DBRTD in the voltage-controlled regime have been studied in [13]. Up to now the DBRTD remains the most prominent example of a semiconductor system which experiences such a characteristic. Our main conclusions, however, may be applied to more general cases of an extended system with a Z-shaped bistability.

The paper is organized as follows. In Sec. II we study the case of a voltage-driven control circuit where the switching front propagates in a self-similar way. Here we establish an approximate analytical dependence of the front velocity on the control potential and compare it with the results of numerical simulations. Section III is devoted to the effect of a global constraint on front dynamics. We demonstrate that this constraint can provide both positive and negative feedback and allows for tuning between accelerated, decelerated, and oscillating fronts. A stability analysis of stationary fronts in the presence of a global constraint is performed in the Appendix.

II. SELF-SIMILAR FRONT PROPAGATION

Let us consider the case of a voltage-driven control circuit $u=$const first. The dynamics is then governed by Eq. (5) with fixed external parameters u and U in the local kinetic function $f(a,u,U)$. Therefore a transition from the off state into the on state (via a propagating *hot front*) or from the on state into the off state (via a propagating *cold front*) occurs with a constant speed v and a self-similar profile $a(x,t)=a_0(x-vt)$; it represents the nonequilibrium phase transition from a metastable state to a stable state [1,38]. Here we assume $v>0$ and $v<0$ for hot and cold fronts, respectively. Front propagation in *pnpn* structures was first described as an autowave in bistable media in [27]. In the comoving frame Eq. (5) takes the form

$$a_0''+va_0'+f(a_0,u,U)=0 \tag{8}$$

and the required front solution with

$$a_0(x)\to a_{\rm on},a_{\rm off} \quad \text{for } x\to-\infty,+\infty \tag{9}$$

corresponds to a saddle-to-saddle trajectory (heteroclinic orbit) in the corresponding phase portrait. In this section we will establish the dependence of the front velocity v and the front width W upon the control potential u.

A general expression for the front velocity can be derived by multiplying Eq. (8) by a_0' and integrating over $\int_{-\infty}^{+\infty}dx$ [1]:

$$v=A\left[\int_{-\infty}^{+\infty}\left(\frac{da_0(x)}{dx}\right)^2dx\right]^{-1},\quad A\equiv\int_{a_{\rm off}}^{a_{\rm on}}f(a,u,U)da. \tag{10}$$

The front has zero velocity if the equal areas rule $A=0$ [2] holds. Without loss of generality we assume that the main voltage U is fixed at the value $U=U_{\rm co}$ which is given by the equal areas rule $\int_{a_{\rm off}}^{a_{\rm on}}f(a,u=0,U_{\rm co})=0$ corresponding to zero control voltage. Then for $u=0$ the front represents a stationary kink.

To further evaluate the dependence $v(u)$ we take into account the specific features of the local kinetic function (2) (Fig. 2) and the resulting $a(u)$ dependence [Fig. 3(a)] and assume: (a) in the interval $[a_{\rm off},a_{\rm int}]$ the local kinetic function is approximately linear and given by $f(a,u,U)\approx-\alpha a+\gamma U+\kappa u$; (b) $(a_{\rm on}-a_{\rm int})\ll(a_{\rm int}-a_{\rm off})$, where $a_{\rm on}$, $a_{\rm off}$, and $a_{\rm int}$ denote the on, off, and intermediate stationary states, respectively; (c) $a_{\rm on}$ and $a_{\rm int}$ essentially do not depend on the gate potential u [Fig. 3(a)], and $a_{\rm off}(u)$ is given by $a_{\rm off}=\tilde{a}_{\rm off}+(\kappa/\alpha)u$, where $\tilde{a}_{\rm off}=(\gamma/\alpha)U$ corresponds to $u=0$.

Because of assumption (a) Eq. (8) has an explicit solution in the interval $[a_{\rm off},a_{\rm int}]$:

$$a_0(x)=a_{\rm off}+(a_{\rm int}-a_{\rm off})\exp[-x/L(v)],$$

$$L(v)^{-1}\equiv\frac{v}{2}+\sqrt{\frac{v^2}{4}+\alpha}. \tag{11}$$

Here $L(v)$ is a characteristic length governing the front width W (see Fig. 4) whose scale is given by $\alpha^{-1/2}$. Due to assumption (b) the contribution of the interval $[a_{\rm int},a_{\rm on}]$ to the front width is small. Therefore we can neglect the contribution of the corresponding interval $[-\infty,0]$ on the x axis

to the integral in Eq. (10). (This means that for the interval $[a_{\rm int},a_{\rm on}]$ the second term in Eq. (8) can be neglected.) Approximating

$$\int_{-\infty}^{+\infty}\left(\frac{da_0(x)}{dx}\right)^2 dx \approx \int_{0}^{+\infty}\left(\frac{da_0(x)}{dx}\right)^2 dx \qquad (12)$$

and inserting Eq. (11) into Eq. (10), by direct calculation we obtain an expression which determines the velocity and the width of the front:

$$\frac{v}{2}+\sqrt{\frac{v^2}{4}+\alpha}=L(v)^{-1}=\frac{\sqrt{2\Delta}}{a_{\rm on}-a_{\rm off}}, \qquad (13)$$

where

$$\Delta\equiv\int_{a_{\rm int}}^{a_{\rm on}} f(a,u,U)da = A+\frac{1}{2}\alpha(a_{\rm int}-a_{\rm off})^2. \qquad (14)$$

Here we have neglected the difference between $a_{\rm on}$ and $a_{\rm int}$. This expression is valid for both hot and cold fronts. With increasing absolute value of the front velocity $|v|$ the front width W decreases or increases for hot ($v>0$) or cold ($v<0$) fronts, respectively.

For slow fronts ($|v|\ll\sqrt{\alpha}$), Eq. (11) gives $L^{-1}(v)\approx v/2+\sqrt{\alpha}$. Equation (13) can be linearized with respect to $v/\sqrt{\alpha}$. This yields

$$v=\frac{2A}{\sqrt{\alpha}(a_{\rm on}-a_{\rm off})^2}. \qquad (15)$$

For fast hot fronts ($v\gg\sqrt{\alpha}$), Eq. (11) yields $L^{-1}\approx v$ and $A\approx\Delta$ holds. Equation (13) is equivalent to the well-known expression [1]

$$v=\frac{\sqrt{2A}}{a_{\rm on}-a_{\rm off}} \qquad (16)$$

originally derived in [39] for combustion fronts. For fast cold fronts ($v<0$, $|v|\gg\sqrt{\alpha}$, $|A|\gg\Delta$) linearization of Eq. (13) with respect to $\sqrt{\alpha}/|v|$ leads to the formula

$$v=-\sqrt{\frac{|A|}{\Delta}}, \qquad (17)$$

which is specific for the local kinetic function (2).

We shall now use Eq. (13) to determine the dependence $v(u)$. The dependence of Δ upon u,

$$\Delta(u)=\Delta(0)+\kappa(a_{\rm on}-a_{\rm int})u,$$
$$\Delta(0)=\exp a_{\rm on}-\exp a_{\rm int}-\frac{1}{2}\alpha(a_{\rm on}^2-a_{\rm int}^2) \qquad (18)$$
$$+\alpha(a_{\rm on}-a_{\rm int})\tilde{a}_{\rm off},$$

is weak due to $a_{\rm on}-a_{\rm int}\ll a_{\rm on}-a_{\rm off}$. Assuming $\Delta(u)\approx\Delta(0)$ we conclude that the front velocity is mainly determined by the front contrast $h\equiv a_{\rm on}-a_{\rm off}$:

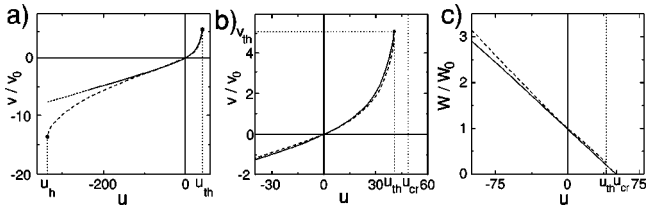

FIG. 5. (a),(b) Front velocity v and (c) front width W as a function of the gate potential u for self-similar front propagation (v and W are normalized by the characteristic velocity $v_0\equiv\sqrt{\alpha}$ and the width W_0 of the stationary front at $u=0$, respectively, u is in units of kT/e). In (b) a part of (a) is shown in an enlarged scale. The numerical result and the analytical approximation are plotted by dashed and solid lines, respectively.

$$\frac{v}{2}+\sqrt{\frac{v^2}{4}+v_0^2}=v_0\frac{h_0}{h}, \quad v_0\equiv\sqrt{\alpha}, \qquad (19)$$

where $h_0=a_{\rm on}-\tilde{a}_{\rm off}$ corresponds to the stationary front at $u=0$. In order to eliminate $\Delta(0)$ from Eq. (19) we have taken into account that $v=0$ for $h=h_0$. Equation (19) determines the dependence of the front velocity on front contrast $v(h)$ in an implicit form. The characteristic speed v_0 sets the scale of the front velocity.

Now let us derive the $v(u)$ dependence. Taking into account assumption (c) [$a_{\rm off}=\tilde{a}_{\rm off}+(\kappa/\alpha)u$ and $a_{\rm on}\approx$const] we obtain

$$\frac{v}{2}+\sqrt{\frac{v^2}{4}+v_0^2}=v_0\left(1-\frac{u}{u_{\rm cr}}\right)^{-1}, \qquad (20)$$

where $u_{\rm cr}\equiv(\alpha/\kappa)h_0$ corresponds to the point where the extrapolated off branch intersects the on branch of the $a(u)$ characteristic [Fig. 3(a)]. Since $u_{\rm cr}$ exceeds the threshold voltage $u_{\rm th}$ Eq. (20) is valid only within the bistability regime $u<u_{\rm th}$. For small values of u the $v(u)$ dependence is given explicitly by

$$v(u)=2v_0\frac{u}{u_{\rm cr}} \quad \text{for } |v|\ll v_0. \qquad (21)$$

In Figs. 5(a) and 5(b) the front velocity $v(u)$ given by Eq. (20) (solid line) is compared with the dependence obtained from direct numerical simulations of the front propagation (dashed line). There is good agreement in the interval $u_h/2<u<u_{\rm th}$. The significant discrepancy for $u_h<u<u_{\rm th}/2$ results from the violation of the assumption $\Delta(u)\approx\Delta(0)$ for fast cold fronts. The threshold points u_h and $u_{\rm th}$ correspond to the degenerate situations where the metastable state $a_{\rm on}$ or $a_{\rm off}$, respectively, merge with the unstable state $a_{\rm int}$. The corresponding velocities $v(u_h)$ and $v(u_{\rm th})$ are maximum velocities of cold and hot fronts, respectively. Numerical simulations show that $|dv(u)/du|=\infty$ at $u=u_h$, $u_{\rm th}$ which is not predicted by Eq. (20). However, we conclude that in the most interesting range of control parameters u Eq. (20) describes the velocity of both hot and cold fronts within good accuracy. According to Eqs. (13) and (20) the front width W is proportional to the deviation of the control potential from

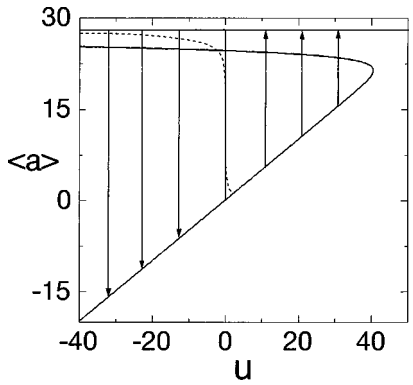

FIG. 6. The phase flow in the $(\langle a\rangle,u)$ plane for self-similar front propagation in the voltage-driven regime. The thick solid line shows the null isocline $a(u)$ of spatially uniform solutions [cf. Fig. 3(a)]. The thin solid line at $u=0$ represents a branch of stationary fronts for $\mathcal{L}\gg W$; the dashed line corresponds to stationary fronts for finite system size ($\mathcal{L}=2W_0$). (a and u are in units of kT/e.)

the critical value $u_{\rm cr}$: $W\sim(u_{\rm cr}-u)$. This prediction is also confirmed by numerical simulations for the interval $u_h/2<u<u_{\rm th}$ [Fig. 5(c)].

In the $(\langle a\rangle,u)$ phase plane the trajectories corresponding to the self-similar front propagation are represented by straight vertical arrows (Fig. 6). The phase flow is directed up towards the on state (hot fronts) and down towards the off state (cold fronts) for $u>0$ and $u<0$, respectively. For $\mathcal{L}\gg W$ the line $u=0$ corresponds to $v=0$ (stationary kinks). In finite-size systems the branch of stationary kinks slightly deviates from the vertical direction in such a way that $\langle a\rangle$ decreases as u increases. That leads to the instability of stationary kinks with respect to infinitesimal fluctuations in the current-controlled regime. The detailed stability analysis of stationary kinks in the presence of a global constraint is given in the Appendix.

III. GLOBALLY COUPLED DYNAMICS OF FRONT PROPAGATION

A. Regimes of the load line

Generally, the average value $\langle a\rangle$ depends on the front position w and due to the global constraint the control parameter u changes as the front propagates. That leads to acceleration or deceleration of the front motion. We shall discuss this in the $(\langle a\rangle,u)$ phase plane. The null isocline corresponding to Eq. (6) is given by

$$\langle a\rangle=\frac{1+\omega}{\omega}\,u-\frac{u_0}{\omega}. \tag{22}$$

It is equivalent to the *load line*

$$\langle j\rangle=\frac{\sigma}{\omega}\,(u_0-u)=\frac{u_0-u}{R\mathcal{L}} \tag{23}$$

in the $(\langle j\rangle,u)$ plane, observing Eq. (4). The intersection points of the load line with the steady-state characteristic $\langle a(u)\rangle$ [resulting from $a''+f(a,u,U)=0$] determine the fixed points of the system. For *bistable* regimes which are relevant for front propagation the null isocline (22), i.e., the load line, should intersect both the on and off branches of the spatially homogeneous $a(u)$ dependence given by $f(a,u,U)=0$. We distinguish three different situations $\omega>0$, $-1<\omega<0$, and $\omega<-1$ where the null isocline has positive, negative, and again positive slope, respectively. These null isoclines and the corresponding positions of the load line with respect to the Z-shaped current-voltage characteristic are shown in Fig. 7. For $\omega<0$ the load resistance R is negative. This can be achieved by implementation of an active external circuit [11]. The total resistivity of the gate circuit $(R+r)$ is positive for $-1<\omega<0$ and negative for $\omega<-1$. For $\omega=0$ and $\omega=\infty$ we have voltage- and current-controlled conditions, respectively. According to Eq. (6) for fixed $\langle a\rangle$ the variable u tends to the quasistationary value given implicitly by Eq. (22) for $\epsilon>0$ if $\omega>-1$ and for $\epsilon<0$ if $\omega<-1$. In this case the null isocline (22) attracts trajectories in the $(\langle a\rangle,u)$ plane. In the opposite case of repulsion the dynamics of our model becomes unbounded. Physically, the case of repulsion corresponds to the regimes of homogeneous oscillations induced by negative external resistance R which are of no interest with respect to the front propagation. It should be noted that in order to exclude such oscillations for $-1<\omega<0$ one should provide a negative capacitance $C<0$ as well (see [11,40,31]), whence $\epsilon\equiv RC/\tau_a>0$.

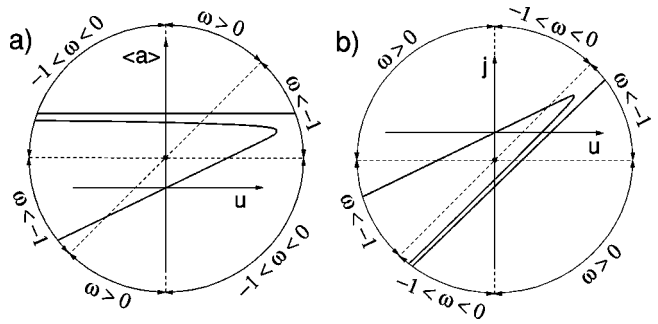

FIG. 7. Different regimes of the load line. (a) The slope of the null isocline (22) of the control voltage u in the $(\langle a\rangle,u)$ phase plane for different values of ω (load resistance). The sectors corresponding to $\omega>0$, $-1<\omega<0$, and $\omega<-1$ are marked by arrows on the circular boundary. The dotted lines separating these different regimes correspond to the respective null isoclines $\langle a\rangle=u+\text{const}(\omega=\pm\infty)$, $\langle a\rangle=u_0(\omega=-1)$, and $u=u_0(\omega=0)$. Note that for a fixed value of ω a null isocline may be shifted vertically by changing u_0. The thick solid lines show the spatially homogeneous steady-state characteristic. (b) The corresponding position of the load line with respect to the Z-shaped current-voltage characteristic in the (j,u) phase plane. The inclined dotted line is parallel to the lowest (*on*) branch of the current-voltage characteristic.

B. Reduction of the equations of motion

An analytical insight into nonlocal dynamics can be achieved by a reduction of the equations of motion (5), (6). Let us parametrize a propagating front by its position $w(t)$ and its contrast $h(t)\equiv a_{\rm on}-a_{\rm off}(t)$. Since in large systems the relaxation of the front shape is fast compared to the front motion, the front dynamics can be described by ordinary differential equations for these reduced order parameters [41], together with the global constraint:

$$\dot{w} = v(h), \tag{24}$$

$$\dot{h} = \alpha(h_0 - h) - \kappa u, \tag{25}$$

$$\epsilon \dot{u} = u_0 - (1+\omega)u + \omega\left(a_{\mathrm{on}} - h + h\,\frac{w}{\mathcal{L}}\right). \tag{26}$$

Equation (24) determines the front velocity according to Eq. (19). Equation (25) describes the relaxation of the front contrast. As in our model $a_{\mathrm{on}} = \mathrm{const}$ this relaxation is related to the relaxation of the homogeneous off state only and therefore Eq. (25) follows directly from Eq. (5). Equation (26) represents the global constraint (6) where $\langle a \rangle$ is expressed through w and h. The contribution of the front wall to $\langle a \rangle$ is neglected. Following [41] we refer to Eqs. (24)–(26) as to *reduction (i)*.

Further simplification of the equations of motion can be achieved if the relaxation of the contrast h is fast compared to the front propagation. It follows from Eq. (24) that the time scale for h is α^{-1}. The time scale for w refers to the time it takes for the front to advance by its own width W. Taking into account that the characteristic front width is $\alpha^{-1/2}$ we arrive at the condition $|v| \ll v_0 \equiv \sqrt{\alpha}$. Therefore we can expect that for sufficiently low velocities the variable h in the dynamical system (24)–(26) can be considered as a fast variable. Generally, that might result either in a situation where this variable can be *adiabatically eliminated* [the contrast $h(t)$ is close to that of the quasistationary front corresponding to the instantaneous value of u] or in a situation where *fast motion* related to this variable dominates the dynamics of the other variables. In order to check whether such fast motion occurs in our system let us consider reduction (i) for $\epsilon \ll \alpha^{-1}$ when there is no delay in the response of the control potential to the momentary value of $\langle a \rangle$. Then eliminating u adiabatically, we arrive at what will be called *reduction (ii)*:

$$\dot{w} = v(h), \tag{27}$$

$$\dot{h} = \kappa\left((u_{\mathrm{cr}} - u_a) - Bh - Ah\,\frac{w}{\mathcal{L}}\right), \tag{28}$$

where

$$u_a \equiv \frac{\omega}{\omega+1}\left(a_{\mathrm{on}} + \frac{u_0}{\omega}\right), \quad A \equiv \frac{\omega}{\omega+1}, \quad B \equiv \frac{\alpha}{\kappa} - \frac{\omega}{\omega+1}. \tag{29}$$

The potential u_a corresponds to the point where the load line intersects the on branch of the $a(u)$ characteristic. The null isocline (22) in the $(\langle a \rangle, u)$ plane (Fig. 7) has positive or negative slope for $A>0$ or $A<0$, respectively. The parameter B controls the slope of the null isocline (22) relative to the slope of the off branch $a_{\mathrm{off}}(u) = \tilde{a}_{\mathrm{off}} + (\kappa/\alpha)u$. (Note that due to $\alpha/\kappa > 1$ the latter slope never exceeds unity.)

The null isoclines in the (h,w) phase plane are explicitly given by $h = h_0$ for Eq. (27) and

$$h = \frac{u_{\mathrm{cr}} - u_a}{A\ \ (w/\mathcal{L}) + B} \tag{30}$$

for Eq. (28). Taking into account Eq. (29) and $a_{\mathrm{on}} - a_{\mathrm{int}} \ll a_{\mathrm{on}} - a_{\mathrm{off}}$ we conclude that the following four combinations of signs of A, B, $(u_{\mathrm{cr}} - u_a)$ are possible:

$$(A>0,\ B>0,\ u_{\mathrm{cr}} - u_a > 0)$$

$$\text{for } \omega > 0 \text{ and for } \omega < -\frac{\alpha}{\alpha - \kappa}, \tag{31}$$

$$(A<0,\ B>0,\ u_{\mathrm{cr}} - u_a > 0) \qquad \text{for } -1 < \omega < 0, \tag{32}$$

$$(A>0,\ B<0,\ u_{\mathrm{cr}} - u_a > 0)$$

$$\text{for } -\frac{\alpha}{\alpha - \kappa} < \omega < -1 \quad \text{if } u_0 > (1+\omega)u_{\mathrm{cr}} + \omega a_{\mathrm{on}}, \tag{33}$$

$$(A>0,\ B<0,\ u_{\mathrm{cr}} - u_a < 0)$$

$$\text{for } -\frac{\alpha}{\alpha - \kappa} < \omega < -1 \quad \text{if } u_0 < (1+\omega)u_{\mathrm{cr}} + \omega a_{\mathrm{on}}. \tag{34}$$

Standard phase portrait analysis in the (w,h) plane shows that the variable h rapidly relaxes to the null isocline (30) for the cases (31)–(33). This implies that asymptotically all motion occurs along the null isocline (30). For case (34) the component of the phase flow related to the variable h changes its direction and the null isocline (30) does not attract the phase flow anymore. The fixed point corresponding to a stationary front is a saddle point and the null isocline (30) closely approximates the stable manifold of this fixed point. Fast dynamics of the variable h driving the system away from this manifold is expected in this case. The case (34) corresponds to a specific position of the load line (23) where it has one intersection with the off branch of the current-voltage characteristic within the bistable region and another intersection with the on branch at $u_a > u_{\mathrm{cr}}$. We will discuss the front dynamics for this regime in detail in Sec. III F.

The analysis above indicates that the variable h can be adiabatically eliminated in all regimes of global coupling except for case (34). Since the contrast $h(t)$ is close to that of the quasistationary front corresponding to the instantaneous value of u the front velocity is determined by the value of u and we can use the dependence (20) instead of Eq. (19). In this case reduction (i) results in the following two-component model [referred to as *reduction (iii)*]

$$\dot{w} = v(u), \tag{35}$$

$$\epsilon \dot{u} = \omega\left[\frac{u_a - u}{A} - \frac{\kappa}{\alpha}\left(1 - \frac{w}{\mathcal{L}}\right)(u_{\mathrm{cr}} - u)\right]. \tag{36}$$

Here $v(u)$ is the velocity of a quasistationary propagating front for the control voltage u, and $h(u) = h_0 - (\kappa/\alpha)u$ has been taken into account.

In the following we compare the predictions of the reductions (i) and (iii) with the results of numerical simulations of the full model (5), (6).

C. Feedback on front dynamics for different types of global coupling

In this subsection we discuss the different types of feedback upon front dynamics occurring for different regimes of the load line. First let us use reduction (iii) and consider the additional assumption $\epsilon \ll \alpha^{-1}$ where there is no delay in the response of the control potential u to the front position. Then Eq. (36) directly determines the instantaneous dependence of u on the front position w. Substituting this dependence into Eq. (20) we obtain the following dependence of the front velocity v on the front position w:

$$\frac{v}{2}+\sqrt{\frac{v^2}{4}+v_0^2}=v_0\,\frac{u_{\mathrm{cr}}}{u_{\mathrm{cr}}-u_a}\left(A\,\frac{w}{\mathcal{L}}+B\right)\frac{\kappa}{\alpha}. \qquad (37)$$

[The same result follows from reduction (ii) by substituting Eq. (30) into Eq. (19).] Equation (37) allows one to understand what kind of feedback occurs for different slopes of the null isocline. It is readily seen that the type of feedback is governed by the sign of the product $\delta \equiv (u_{\mathrm{cr}}-u_a)A$. For $u_a < u_{\mathrm{cr}}$ we get $\mathrm{sgn}\,\delta = \mathrm{sgn}\,A$, and the feedback is positive or negative for positive or negative slope of the null isocline, respectively, i.e., the front velocity v increases or decreases, respectively, with increasing $w(t)$. For $u_a > u_{\mathrm{cr}}$ the reverse holds. The front propagates with acceleration and deceleration for $\delta > 0$ and $\delta < 0$, respectively. According to Eq. (37) for $|v| \ll v_0$ or $v \gg v_0$ the front velocity v increases linearly with the front position w which indicates the exponential character of the front propagation.

In the opposite limit case of slow relaxation of the control potential $\epsilon \gg \alpha^{-1}$ the front propagates with a constant speed given by the initial value of u for any global constraint.

In order to understand the front dynamics for intermediate values of ϵ, as well as to study the limits of the reduced two-component model (35), (36), we have performed numerical simulations of the full model (5), (6). Obviously, the analysis of front propagation requires specific initial conditions. We assume that the initial distribution $a_i(x)$ is a steplike pattern: $a_i(x)=a_{\mathrm{on}}$ for $x<x_i$; $a_i(x)=a_{\mathrm{off}}(u_i)$ for $x>x_i$, where x_i and u_i are initial front position and initial gate voltage, respectively. In the absence of global constraints such a steplike pattern is known to evolve exponentially fast into a smooth front profile traveling at constant velocity [38,42,43]. In the following we focus only on regimes which are associated with front propagation and assume that the initial point $(\langle a_i(x)\rangle, u_i)$ is located sufficiently close to the null isocline. Physically, different initial conditions can be realized by means of the lateral gates G_1, G_2.

Now let us discuss the front dynamics for different types of global constraints in detail.

D. Positive feedback ($\omega > 0$)

In the case of positive load resistance R ($\omega > 0$) the parameters A and B are always positive. $B>0$ means that the slope of the null isocline (22) is larger than that of the off branch of the $a(u)$ characteristic. Therefore $u_a < u_{\mathrm{cr}}$ holds for any null isocline which intersects both the on and the off branch of the $a(u)$ characteristic [see Eq. (31)]. According to Eq. (37) we have positive feedback and acceleration of the front. Numerical simulations of the full model (5), (6) are shown in Fig. 8 for three different positions of the load line [dotted in Fig. 8(a)] and different initial conditions. The front velocity v and the relative deviation of the contrast from its quasistationary value h are shown as a function of time in Figs. 8(b) and 8(c), respectively. Trajectory 1 ($u_0>0$) corresponds to an accelerated hot front starting close to the off state and ending in the homogeneous on state [Fig. 8(d)]. Trajectory 4 belongs to a load line with lower $u_0<0$; it corresponds to a cold front starting close to the on state and ending in the off state [Fig. 8(e)]. In the case of $\tilde{a}_{\mathrm{off}} < (-u_0/\omega) < a_{\mathrm{on}}$ [the middle load line in Fig. 8(a)] there is an intersection point of the load line (null isocline) with the branch of stationary fronts at $u=0$. This point corresponds to a stationary kink solution. Linear stability analysis (see the Appendix) indicates a saddle-type instability of this kink solution for $\omega>0$, $\epsilon>0$. Accelerated hot ($v>0$) and cold ($v<0$) fronts predicted by Eq. (37) for $\tilde{a}_{\mathrm{off}} < (-u_0/\omega) < a_{\mathrm{on}}$ represent motion along the unstable manifolds of this saddle point [trajectories 2 and 3, respectively, in Fig. 8(a)]. The feedback is most efficient for the current-controlled regime ($\omega \gg 1$) in the control circuit. An increase of ϵ as it occurs with an increase of the capacitance C results in a delay of the control potential response upon the front position and therefore the front acceleration is diminished [trajectories $1',2',3',4'$ in Fig. 8(a)]. For large values of ϵ we return to

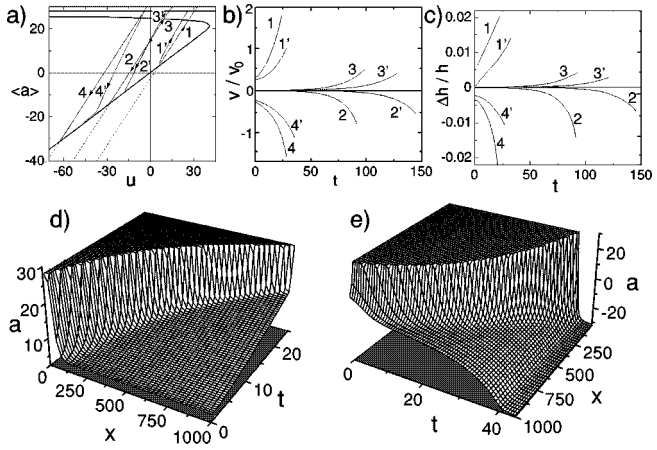

FIG. 8. Propagation of accelerated fronts in the case of positive feedback $\omega>0$ ($R>0$). (a) Phase trajectories in the $(\langle a\rangle, u)$ plane (solid lines with arrows). The thick solid lines show the spatially homogeneous steady-state characteristics. Numerical simulations are shown for three different load lines (dotted) corresponding to $\omega=100$ (nearly current controlled) and $u_0=200, -1500, -3200$. Two different values of $\epsilon \equiv RC/\tau_a$ are used: $\epsilon=10^{-9}$ (trajectories 1,2,3,4) and $\epsilon=5\times10^{-9}$ (trajectories $1',2',3',4'$). Slightly different initial conditions are employed for trajectories 2,2′ and 3,3′, respectively. (b) Front velocity v normalized by v_0 as a function of time for the trajectories presented in (a). (c) Relative deviation of the front contrast from its quasistationary value h as a function of time for the trajectories presented in (a). (d) Temporal evolution of the accelerated hot front corresponding to trajectory 1. (e) Temporal evolution of the accelerated cold front corresponding to trajectory 4. Note that the orientation of axes in (d) and (e) has been chosen differently for better visualization. Numerical parameters as in Fig. 2. (a,u are in units of kT/e, x and t in units of l and τ_a, respectively.)

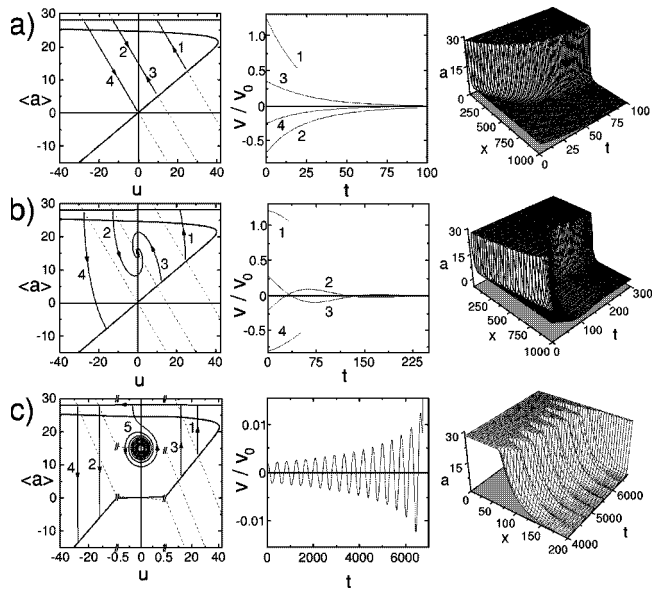

FIG. 9. Front propagation in the case of negative feedback $-1<\omega<0$ $(-r<R<0)$. Numerical simulations are shown for three different load lines (dotted) corresponding to $\omega=-0.5$ and $u_0=20$ (trajectory 1), $u_0=8$ (trajectories 2,3,5), $u_0=0$ (trajectory 4). Three values of ϵ are used: (a) $\epsilon=10^{-11}$, (b) $\epsilon=10^{-8}$, (c) $\epsilon=10^{-6}$. The left column shows the phase trajectories in the $(\langle a\rangle,u)$ plane. Throughout (a),(b),(c), trajectories labeled with the same number are calculated with the same load lines and the same initial conditions. Trajectory 5 in (c) corresponding to an oscillatory instability of the stationary front is calculated with $\omega=-0.95$. Note that in (c) the scale on the u axis has been expanded in the interval $[-0.5,0.5]$ in order to make these oscillations visible. The center column shows the front velocity v normalized by v_0 as a function of time. The right column shows the temporal evolution of fronts: (a) monotonic and (b) oscillatory slowing down of the front propagation corresponding to trajectory 3; (c) growing oscillation corresponding to trajectory 5. (a,u are in units of kT/e, x and t in units of l and τ_a, respectively.)

the case of self-similar front propagation with a constant speed since u does not change appreciably. The deviation of the actual front contrast $h(t)$ from the quasistationary value $h(u(t))$ corresponding to the instantaneous value of u is negligible [Fig. 8(c)]. This justifies reduction (iii) in that particular case. The agreement with the full model (5), (6) is very good.

E. Negative feedback $(-1<\omega<0)$

The case $-1<\omega<0$ corresponds to a negative external resistance $R<0$ whose absolute value does not exceed the internal resistance r so that the total resistance of the gate contact and external load remains positive. Here we have a negative slope of the null isocline $A<0$, and $B>0$, $u_a<u_{\rm cr}$ holds [see Eq. (32)]. Due to $\delta<0$ the feedback is negative and fronts propagate with deceleration [Fig. 9(a)]. The final state depends on the particular position of the null isocline (22). For $-u_0/\omega>a_{\rm on}$ and $-u_0/\omega<a_{\rm off}$ the final state is the on and off state, respectively (trajectories 1 and 4, respectively). For $a_{\rm off}<(-u_0/\omega)<a_{\rm on}$ the system eventually approaches the stationary kink pattern at $u=0$ (trajectories 2 and 3). Stability of the stationary kink for $\epsilon>0$ is given by the criterion (A8), which can be approximately represented as

$$-1+\epsilon\lambda_1<\omega<-\frac{\lambda_1}{\kappa}, \tag{38}$$

where $\lambda_1>0$ is the eigenvalue of the only unstable eigenmode related to the kink solution (see the Appendix). Since $\lambda_1\ll 1$ for $\mathcal{L}\gg W$, this criterion is close to $-1<\omega<0$ for small ϵ. If ω lies in the interval given by Eq. (38), the fixed point corresponding to the stationary kink is a stable node or stable focus for $\epsilon>0$. In the first case, the slowing down of a front is monotonic [Fig. 9(a)], in the second case we find an oscillatory slowing down [Fig. 9(b)]. The lower bound of the criterion (38) corresponds to an oscillatory instability: for $\omega<-1+\epsilon\lambda_1$ the fixed point is an unstable focus. This instability results in growing oscillations of the front position [Fig. 9(c), trajectory 5]. The amplitude of these oscillations increases monotonically. We have never observed limit-cycle oscillations of the front position in our numerical simulations. Eventually the front reaches the boundary. Starting from this point the system remains in the subspace of spatially homogeneous solutions and its dynamics depends on whether the null isocline intersects the on or off branch of the $a(u)$ characteristic. If it does, the system eventually approaches the nearest homogeneous fixed point as shown in Fig. 9(c) (curve 5). Otherwise the front oscillations evolve into homogeneous oscillations. The oscillatory instability of a stationary front originates from the attraction of a front by the boundaries [31] that takes place in the voltage-controlled regime $u=$const and is reflected by the positiveness of the eigenvalue λ_1. Note that λ_1 decreases exponentially with system size $\mathcal{L}$ and in an infinite system $\lambda_1=0$ due to the translation invariance. Therefore the oscillatory instability essentially represents a boundary effect which is not typical for fronts on large spatial domains. The deviation of the front contrast h from its quasistationary value is small for all regimes. However, since reduction (iii) does not include boundary effects it cannot describe the oscillatory instability [Fig. 9(c), trajectory 5].

F. Indeterminate feedback $(\omega<-1)$

For $\omega<-1$ the slope of the null isocline (22) becomes positive again $(A>0)$. In this situation we should compare it with the slope κ/α of the off branch of the $a(u)$ characteristic distinguishing between the situation $B>0$ and $B<0$ (Fig. 10). For $B>0$ [see Eq. (31)] the null isocline (load line) intersects both the on and the off branch of the $a(u)$ characteristic (Fig. 10, curve 1), $u_a<u_{\rm cr}$ holds, and the system dynamics is qualitatively the same as for the positive load $\omega>0$: The feedback is positive and the fronts propagate with acceleration. If the load line intersects the stationary kink solution at $u=0$ this kink exhibits a saddle-type instability if $\epsilon<0$ (see the Appendix). The only difference between the cases $\omega>0$ and $\omega<-1$ is that the sign of $\epsilon\equiv RC/\tau_a$ should be reversed in the latter case, but for $C>0$ this occurs automatically if R changes sign. This qualitative similarity becomes a quantitative one for the current-controlled regime $|\omega|\gg 1$: For a heavily loaded circuit the sign of the external

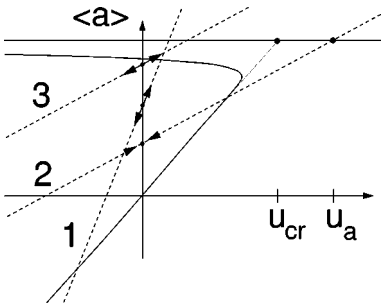

FIG. 10. Possible positions of the load line (dotted) in the $(\langle a\rangle,u)$ phase plane for $\omega<-1$. Line 1 corresponds to $B>0$, lines 2 and 3 to $B<0$. The arrows denote unstable (lines 1, 3) and stable (line 2) manifolds of the saddle point corresponding to the stationary kink. The thick solid lines show the spatially homogeneous steady-state characteristics. The intersection point of the load line with the on state (u_a) is marked for the null isocline 2 only.

resistance does not play a role if the polarity of the voltage source is chosen appropriately.

For $B<0$ $[-\alpha/(\alpha-\kappa)<\omega<-1]$ the slope of the null isocline is smaller than that of the off branch. If the null isocline intersects the stationary kink solution at $u=0$, two cases are possible: there is a further intersection either with the off branch of the $a(u)$ characteristic at $0<u<u_{\rm cr}$ (Fig. 10, curve 2), or with the on branch only (Fig. 10, curve 3). [Curves 2 and 3 correspond to the cases (34) and (33), respectively]. Since there is no intersection for $u<0$, the system dynamics may become unbounded, i.e., unphysical, for $u<0$, therefore in the following we restrict our consideration to $u>0$.

For $B<0$ and $u_a<u_{\rm cr}$ the null isocline intersects the on branch only. Since $\delta=(u_{\rm cr}-u_a)A>0$ we expect positive feedback. For $u>0$ the system dynamics is qualitatively similar to the case $B>0$. In particular, a stationary kink at $u=0$ experiences a saddle-type instability for $\epsilon<0$ and the accelerated front predicted by reduction (iii) corresponds to motion along the unstable manifold of the saddle point up to the stable on state (Fig. 10, curve 3). For $B<0$ and u_a sufficiently larger than $u_{\rm cr}$ the null isocline first intersects the off branch of the $a(u)$ characteristic and further on also the on state (Fig. 10, curve 2) implying $\delta=(u_{\rm cr}-u_a)A<0$ and negative feedback. This situation corresponds to the case (34) where fast motion related to the variable h is expected. Here we meet a *new situation* in the $(\langle a\rangle,u)$ phase plane because the decelerated front predicted by reduction (iii) and tending to the stationary kink pattern at $u=0$ now corresponds to motion along the stable manifold of the saddle point. Decelerated fronts have indeed been found numerically as solutions of the full system (5), (6) for carefully chosen initial conditions. The corresponding trajectory in the $(\langle a\rangle,u)$ plane closely follows the null isocline (22) in such a way that u decreases up to the stationary kink state [Fig. 11(a), curve 1]. In the following we refer to this solution as to the *stable kink mode*. However, numerical simulations reveal also the possibility of a qualitatively different motion where the trajectory runs in the opposite direction (*unstable kink mode*) until it reaches the stable on state [Fig. 11(a), curve 2] [45]. Note that the phase portrait in Fig. 11(a) is a projection of a high-dimensional space, and trajectory 2 need not be close to trajectory 1 in this larger phase space. The

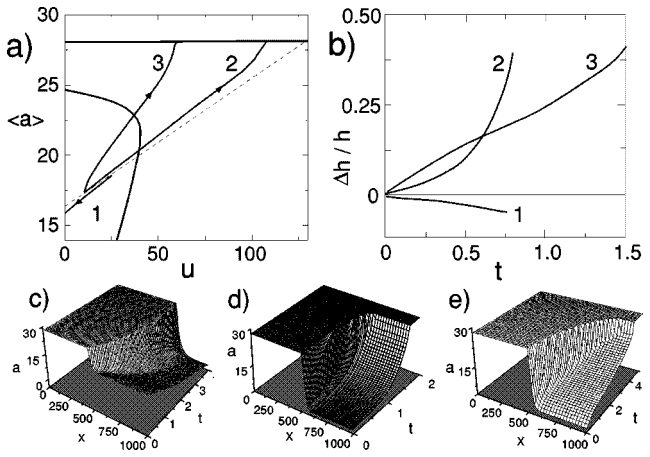

FIG. 11. Front propagation in the case of indeterminate feedback $\omega<-1$ $(R<-r)$. Numerical simulations are shown for a load line corresponding to $\omega=-1.1$ and $u_0=18$ $(u_a>u_{\rm cr}, B<0)$. (a) Phase portrait. The null isocline (dotted) intersects the off branch of the $a(u)$ characteristic (solid line). Trajectories 1 (stable kink mode) and 2 (unstable kink mode) are calculated for $\epsilon=-10^{-12}$. Trajectory 3 corresponds to the same initial condition as 2 but $\epsilon=-5\times10^{-10}$. (b) Relative deviation Δh of the actual front contrast from its quasistationary value h for trajectories 1,2,3 (normalized to h). (c) Temporal evolution of the decelerated hot front corresponding to trajectory 1 (stable kink mode). (d) Temporal evolution of the front corresponding to trajectory 2 (unstable kink mode). (e) Temporal evolution of the accelerated hot front corresponding to trajectory 3 (unstable kink mode with $\epsilon=-5\times10^{-10}$). ($a,u$ are in units of kT/e, x and t in units of l and τ_a, respectively.)

essential difference of the unstable kink mode from the stable kink mode is a significant deviation of the actual contrast $h(t)$ from its quasistationary value $h(u(t))$ [see Fig. 11(b)]. The variable h cannot be adiabatically eliminated and reduction (iii) fails in this case. This confirms our analysis related to reduction (ii) in Sec. III B. An analytical description of the unstable kink mode can be obtained only on the basis of reductions (i) or (ii) which treat the front contrast as an independent variable. This type of feedback is very sensitive to the initial conditions. Generally, the stable or unstable kink mode is favored if the initial condition $\langle a_i(x)\rangle$ lies above or below the null isocline (22), respectively.

The stable and unstable kink modes correspond to decelerated [Fig. 11(c)] and accelerated [Fig. 11(d)] fronts, respectively. However, since the unstable kink mode is triggered by the fast dynamics of the front contrast h, the motion of the front wall is negligible, and the fast change of the contrast makes the major contribution to the dynamics of $\langle a\rangle$ thus driving the system rapidly towards the homogeneous on state [Fig. 11(d)]. This is consistent with the observation that the homogeneous off state is now unstable. With increasing $|\epsilon|$ the unstable kink mode becomes more similar to a well-pronounced accelerated front [Fig. 11(a), curve 3 and Fig. 11(e)]. For the same values of ϵ the stable kink mode cannot be excited anymore: the same initial conditions as in Fig. 11(c) give rise to a mixed motion which starts like a decelerated front but eventually develops into an accelerated one. That means that reduction (iii) becomes completely obsolete with increasing ϵ.

IV. CONCLUSIONS

In this paper we have studied front propagation in a gate-driven semiconductor structure. The system is globally coupled via a gate-cathode circuit which exhibits a Z-shaped bistable current-voltage characteristic. The cathode-anode voltage in the main circuit is fixed and serves as an external parameter which controls the global level of excitation. The type of global constraint and the relaxation time τ_u associated with the global constraint are governed by the load resistance R and the external capacitance $C_{\rm ext}$, respectively.

We have shown that it is possible to arrange either positive or negative feedback upon the front dynamics by global coupling. For $R>0$ the feedback is always positive and both hot and cold fronts propagate with acceleration (Fig. 8). They effect a nonequilibrium phase transition to the homogeneous on or off state, respectively. A negative external load $R<0$ can be introduced by applying an active external circuit. In this case the type of constraint essentially depends on the relation between the external load and the resistance of the gate contact r. For $R+r>0$ the feedback is negative and the front propagates with deceleration. In order to keep the relaxation time τ_u positive and prevent circuit-induced spatially homogeneous relaxation oscillations one should provide also a negative external capacitance in this case. By appropriate choice of the bias voltage u_0 in the control circuit the global constraint can always be tuned such that the decelerated front eventually ends up in a stable stationary kink pattern [Fig. 9(a)]. With increasing τ_u this fixed point is transformed from a stable node [Fig. 9(a)] to a stable focus and the transients take on the form of damped front oscillations [Fig. 9(b)]. Further increase of τ_u leads to an oscillatory instability [Fig. 9(c)]. The critical value of τ_u where the stationary front becomes unstable for any slope of the load line in the interval $-r<R<0$ is given by $\tau_u \approx \tau_a/\lambda_1$, where λ_1 is the eigenvalue of the unstable translation mode related to the stationary kink. The front oscillates with growing amplitude and, as it reaches the boundary, the system switches to the homogeneous mode. Limit-cycle oscillations of the front position, similar to those obtained in [44] for the ballast resistor, do not occur in our model. It is essential that the system remains in a homogeneous state—steady or oscillatory—as far as boundary conditions (determined by the lateral gates G_1, G_2) and global constraint remain unchanged.

All regimes discussed above (except for the oscillatory instability of a stationary front in the case of negative feedback) can be described by a reduced two-component model which treats the front position w and the gate voltage u as dynamical variables and assumes that relaxation of the front contrast and front shape occurs fast compared to the front motion. However, this model fails for $R+r<0$ where both positive and negative feedback upon front dynamics become possible depending on the position of the load line with respect to the current-voltage characteristic. Qualitatively different modes, such as accelerated and decelerated fronts, can be excited for very close-by initial conditions. Whereas decelerated fronts are predicted by the two-component reduced model, the description of accelerated fronts requires at least a reduced model which treats the front contrast as an independent dynamical variable.

Our analysis is applicable to general spatially extended semiconductor systems with a Z-shaped current-voltage characteristic including such quantum devices as the double barrier resonant tunneling diode [11–13]. Self-sustained oscillations of the front position in the DBRTD have been theoretically predicted in [12] for the case of a resonant (second order) external circuit. The analysis in [12] is based on a simplified model and assumes that the oscillation cycle consists of two consecutive stages: front propagation leading to the homogeneous state, and subsequent circuit-induced relaxation of the voltage. During the second stage the device is assumed to be in a homogeneous state. However, it remains unclear how the kink pattern can emerge again from the homogeneous state after the second stage of the oscillation cycle has been completed. Our present analysis provides a thorough understanding of pattern formation in the DBRTD for a realistic first order external circuit and Neumann boundary conditions.

Note that the gate-driven $pnpn$ structure is a three-terminal device which has a Z-shaped cathode-gate current voltage characteristic and an S-shaped cathode-anode characteristic. Generally, such systems should be treated as a bistable medium with two global constraints associated with main and control circuit, respectively, with different nonlinearities. In this paper we have shown that for positive load the gate circuit provides a positive feedback upon the front dynamics. It is well known that the feedback associated with the main circuit is negative. In future work we will study the front dynamics taking both constraints into account and emphasizing the effects which occur due to the interplay between positive and negative feedback.

Our analysis also touches upon some general aspects of front propagation in globally coupled bistable systems. Global coupling has been widely recognized as an important factor which influences and even determines spatiotemporal dynamics in extended systems of different nature [28–30,41,44,46,47]. In particular, accelerated front motion has been found in electrochemical systems [48]. One of the main findings of our analysis reveals that there are regimes where the type of feedback by the global constraint is indeterminate, and both accelerated and decelerated front propagation driving the system to different final states becomes possible for close-by initial values of the front position and the external control parameters.

ACKNOWLEDGMENTS

We are grateful to U. Ebert for enlightening discussions on front propagation into unstable states. P.R. acknowledges financial support from the Alexander von Humboldt Foundation.

APPENDIX

Let us study the stability of a stationary kink $(a_0(x),u_0)$ in the presence of a global constraint. Linearization of Eqs. (5) and (6) with respect to small perturbations $e^{\zeta t}\delta a(x) = a(x,t)-a_0(x)$, $e^{\zeta t}\delta u = u(t)-u_0$ yields

$$\zeta \delta a = \hat{H}_N \delta a + \kappa \delta u, \quad \hat{H}_N \equiv \Delta + \Phi(x), \quad \Phi(x) \equiv \left.\frac{\partial f}{\partial a}\right|_{a_0,u_0}, \tag{A1}$$

$$\epsilon\zeta\,\delta u = -(1+\omega)\,\delta u + \omega\langle \delta a\rangle. \tag{A2}$$

The stationary solution is stable if Re $\zeta<0$ for all eigenvalues ζ.

We denote the eigenfunctions and eigenvalues of the self-adjoint operator $\hat{H}_N$ by $\Psi_i(x)$ and λ_i, respectively. They correspond to the voltage-driven case $u=\text{const}$. The first (ground-state) eigenmode Ψ_1 is strictly positive and corresponds to a shift of the kink wall. For an infinite system ($\mathcal{L}=\infty$) it is given by the Goldstone mode $\Psi_1 = da_0/dx$, and it follows from translation invariance that $\lambda_1=0$. For finite-size systems λ_1 becomes positive due to the attractive action of the boundaries on the kink wall, but all other eigenvalues remain negative [2,31]: $\lambda_1>0$, $\lambda_i<0$ for $i>1$. However, the value of λ_1 decreases exponentially if the ratio $\mathcal{L}/W$ increases and therefore in sufficiently large systems the stationary front has quasineutral stability. In order to study the front stability in the presence of a global constraint we expand the eigenmode $\delta a(x)$ in the basis $\{\Psi_i\}$:

$$\delta a(x) = \sum_m \langle \delta a \Psi_m\rangle \Psi_m\,. \tag{A3}$$

From Eq. (A1) we obtain the coefficients of the expansion (A3). Substituting Eq. (A3) into Eq. (A2) results in the following characteristic equation:

$$F(\zeta) = 1+\omega+\epsilon\zeta-\omega\kappa\sum_m \frac{\langle\Psi_m\rangle^2}{\zeta-\lambda_m} = 0, \tag{A4}$$

which determines the complex eigenvalues ζ of the linearized system (A1), (A2).

The differential conductivity of the kink state

$$\sigma_d \equiv \mathcal{L}\,\frac{d\langle j(a(u),u)\rangle}{du} = \mathcal{L}\left(\left\langle\frac{\partial j}{\partial u}\right\rangle + \left\langle\frac{\partial j}{\partial a}\,\frac{da}{du}\right\rangle\right) \tag{A5}$$

is connected with the eigenvalues λ_i and eigenfunctions Ψ_i by

$$\sigma_d = r^{-1}\left(1+\kappa\sum_m \frac{\langle\Psi_m\rangle^2}{\lambda_m}\right). \tag{A6}$$

Due to $\lambda_1 \ll |\lambda_i|$ and $|\langle\Psi_1\rangle| \gg |\langle\Psi_i\rangle|$ for $i>1$ we neglect all terms except for the first one in the sums in Eqs. (A4) and (A6). Then the characteristic equation (A4) takes the form

$$\epsilon\zeta^2 + \zeta(1+\omega-\epsilon\lambda_1) - \lambda_1(1+\omega\tilde{\sigma}_d) = 0, \quad \tilde{\sigma}_d \equiv \sigma_d r. \tag{A7}$$

From Eq. (A7) we get the following stability criteria:

$$-1+\epsilon\lambda_1 < \omega < -\tilde{\sigma}_d^{-1} \quad \text{if } \epsilon>0, \tag{A8}$$

$$-\tilde{\sigma}_d^{-1} < \omega < -1+\epsilon\lambda_1 \quad \text{if } \epsilon<0. \tag{A9}$$

According to Eq. (A6) $\tilde{\sigma}_d \approx \kappa/\lambda_1$ which means that the differential conductance of a stationary kink is positive and large: $\tilde{\sigma}_d \gg 1$. Therefore neither Eq. (A8) nor Eq. (A9) are met for $\omega>0$. For $\omega>0$, $\epsilon>0$ the fixed point is a saddle point, for $\omega>0$, $\epsilon<0$ it is an unstable focus or unstable node. Since $\tilde{\sigma}_d \gg 1$ we also conclude that the criterion (A9) is never satisfied for $\omega<0$: for $\omega<0$, $\epsilon<0$ the fixed point is a saddle point or, in the narrow interval $-\tilde{\sigma}_d^{-1}<\omega<0$, an unstable node. Stabilization becomes possible only in the case (A8) if $\epsilon>0$ and $\omega<0$.

For small ϵ and $\mathcal{L}\gg W$ (i.e., λ_1, $\tilde{\sigma}_d^{-1}\to 0$) this criterion takes the approximate form $-1<\omega<0$ which coincides with the condition of negative slope of the null isocline (22) of the global constraint (Fig. 7). The upper and lower bounds of condition (A8) correspond to saddle-node and Hopf bifurcations, respectively. It should be noted that in the case $\omega<0$ the load resistance R is negative, and in order to keep $\epsilon \equiv RC/\tau_a$ positive a negative capacitance $C<0$ is required. This is generally necessary to eliminate oscillations induced by a negative external load (see [11,31,40]).

[1] A. S. Mikhailov, *Foundation of Synergetics* (Springer, Berlin, 1994), Vol. 1.

[2] E. Schöll, *Nonequilibrium Phase Transitions in Semiconductors* (Springer, Berlin, 1987).

[3] M. P. Shaw, V. V. Mitin, E. Schöll, and H. L. Grubin, *The Physics of Instabilities in Solid State Electron Devices* (Plenum Press, New York, 1992).

[4] B. S. Kerner and V. V. Osipov, *Autosolitons* (Kluwer Academic Publishers, Dordrecht, 1994).

[5] *Nonlinear Dynamics and Pattern Formation in Semiconductors and Devices*, edited by F.-J. Niedernostheide (Springer, Berlin, 1995).

[6] H. Engel, F.-J. Niedernostheide, H. G. Purwins, and E. Schöll, *Self-Organization in Activator-Inhibitor-Systems: Semiconductors, Gas Discharge, and Chemical Active Media* (Wissenschaft und Technik Verlag, Berlin, 1996).

[7] D. Jäger, H. Baumann, and R. Symanczyk, Phys. Lett. A **117**, 141 (1986).

[8] A. Minarsky and P. Rodin, Pis'ma Zh. Tekh. Fiz. **20**, 38 (1994) [Tech. Phys. Lett. **20**, 490 (1994)]; Fiz. Tekh. Poluprovodn. **31**, 432 (1997) [Semiconductors **31**, 366 (1997)]; Solid-State Electron. **41**, 813 (1997).

[9] A. Wacker and E. Schöll, Semicond. Sci. Technol. **7**, 1456 (1992); Z. Phys. B **93**, 431 (1994).

[10] S. Bose, A. Wacker, and E. Schöll, Phys. Lett. A **195**, 144 (1994).

[11] A. Martin, M. Lerch, P. Simmonds, and L. Eaves, Appl. Phys. Lett. **64**, 1248 (1994).

[12] B. Glavin, V. Kochelap, and V. Mitin, in *Proceedings of the International Conference on Quantum Devices and Circuits*, edited by K. Ismail, S. Bandyopadhyay, and J. P. Leburton (World Scientific, Singapore, 1996).

[13] B. Glavin, V. Kochelap, and V. Mitin, Phys. Rev. B **56**, 13 346 (1997); D. Mel'nikov and A. Podlivaev, Fiz. Tekh. Poluprovodn. **32**, 227 (1998) [Sov. Phys. Semicond. **32**, 206 (1998)].

[14] A. V. Gorbatyuk, I. A. Linijchuk, and A. V. Svirin, Pis'ma Zh.

Tekh. Fiz. **15**, 42 (1989) [Sov. Tech. Phys. Lett. **15**, 224 (1989)].
[15] A. Gorbatyuk and P. Rodin, Pis'ma Zh. Tekh. Fiz. **16**, 519 (1990) [Sov. Tech. Phys. Lett. **16**, 519 (1990)]; Radiotekh. Elektron. **40**, 1876 (1994) [J. Commun. Technol. Electron. **40**, 49 (1995)].
[16] A. Gorbatyuk and P. Rodin, Solid-State Electron. **35**, 1359 (1992); Radiotekh. Elektron. **37**, 910 (1992) [Sov. J. Commun. Technol. Electron. **37**, 97 (1992)].
[17] A. Gorbatyuk and P. Rodin, Z. Phys. B **104**, 45 (1997).
[18] M. Meixner, P. Rodin, and E. Schöll, Phys. Status Solidi B **204**, 493 (1997).
[19] F.-J. Niedernostheide, M. Ardes, M. Or-Guil, and H.-G. Purwins, Phys. Rev. B **49**, 7370 (1994).
[20] F.-J. Niedernostheide, C. Brillert, B. Kukuk, H.-G. Purwins, and H.-J. Schulze, Phys. Rev. B **54**, 14 012 (1996).
[21] A. V. Gorbatyuk and F.-J. Niedernostheide, Physica D **99**, 339 (1996).
[22] F.-J. Niedernostheide, H. J. Schulze, S. Bose, A. Wacker, and E. Schöll, Phys. Rev. E **54**, 1253 (1996).
[23] F.-J. Niedernostheide, M. Or-Guil, M. Kleinkes, and H.-G. Purwins, Phys. Rev. E **55**, 4107 (1997).
[24] A. S. Mikhailov, in *Nonlinear Waves, Dynamics and Evolution*, edited by A. V. Gaponov-Grekhov and M. I. Rabinovich (Springer, Berlin, 1989).
[25] H. Haken, C.-D. Schulz, and M. Schindel, in *Proceedings of the First Conference of Applied Synergetics and Synergetical Engineering, Erlangen, Germany, 1994*, edited by F. G. Boebel and T. Wagner (Fraunhofer Society, Erlangen, 1994).
[26] I. V. Varlamov and V. V. Osipov, Fiz. Tekh. Poluprovodn. **3**, 950 (1969) [Sov. Phys. Semicond. **3**, 803 (1969)].
[27] M. D'yakonov and M. Levinstein, Fiz. Tekh. Poluprovodn. **12**, 729 (1978) [Sov. Phys. Semicond. **12**, 426 (1978)].
[28] F. G. Bass, V. S. Bochkov, and Yu. G. Gurevich, Zh. Eksp. Teor. Fiz. **58**, 1814 (1970) [Sov. Phys. JETP **31**, 972 (1970)].
[29] L. Schimansky-Geier, Ch. Zülicke, and E. Schöll, Z. Phys. B **84**, 433 (1991).
[30] L. Schimansky-Geier, Ch. Zülicke, and E. Schöll, Physica A **188**, 436 (1992).
[31] A. Alekseev, S. Bose, P. Rodin, and E. Schöll, Phys. Rev. E **57**, 2640 (1998).
[32] *Proceedings of the International Symposium on Power Semiconductor Devices, Davos, Switzerland, May 31–June 2, 1994*, edited by W. Fichtner and A. Jaecklin (Hartung-Gorre, Konstanz, 1994).
[33] D. Ruwisch, M. Bode, H. J. Schulze, and F. J. Niedernostheide, in *Nonlinear Physics of Complex Systems*, edited by J. Parisi and W. Zimmermann, Lecture Notes in Physics Vol. 476 (Springer, Berlin, 1996), pp. 194–212.
[34] C. V. Radehaus and H. Willebrand, in Ref. [5], p. 250.
[35] Yu. Balkarei and M. Elinson, Pis'ma Zh. Tekh. Fiz. **17**, 73 (1991) [Sov. Tech. Phys. Lett. **17**, 487 (1991)].
[36] Yu. Balkarei, M. Evtikhov, and M. Elinson, Zh. Tekh. Fiz. **57**, 209 (1987) [Sov. Phys. Tech. Phys. **32**, 127 (1987)].
[37] Generally, Eq. (1) should be treated together with two global constraints related to the main and control circuits, respectively, as done in [17] for an analysis of time-independent patterns. However, since the global constraint associated with the main circuit is known to be inhibiting for a positive load resistance [28,40,31] our system does not exhibit fast motion related to the variable U. This makes the assumption $U = \text{const}$ physically relevant.
[38] E. Ben-Jacob, H. Brand, G. Dee, L. Kramer, and J. S. Langer, Physica D **14**, 348 (1985).
[39] Ya. Zel'dovich and D. Frank-Kamenetskij, Zh. Eksp. Khim. **12**, 100 (1938).
[40] A. Wacker and E. Schöll, J. Appl. Phys. **78**, 7352 (1995).
[41] F. J. Elmer, Phys. Rev. A **41**, 4174 (1990).
[42] W. van Saarlos, Phys. Rev. A **37**, 211 (1988); **39**, 6367 (1989).
[43] U. Ebert and W. van Saarlos, Phys. Rev. Lett. **80**, 1650 (1998).
[44] F. J. Elmer, Z. Phys. B **87**, 377 (1992).
[45] Note that the terms *stable* and *unstable* in this case refer to the respective manifolds in phase space.
[46] D. Battogtokh and A. S. Mikhailov, Physica D **90**, 84 (1996).
[47] M. Falcke, H. Engel, and M. Neufeld, Phys. Rev. E **52**, 98 (1995).
[48] N. Mazouz, G. Flätgen, and K. Krischer, Phys. Rev. E **55**, 2260 (1997).